Monthly Notices
of the
ROYAL ASTRONOMICAL SOCIETY

MNRASL **434,** L16–L20 (2013)
Advance Access publication 2013 June 11

doi:10.1093/mnrasl/slt069

Stacked reverberation mapping

S. Fine,[1]⋆ T. Shanks,[2] P. Green,[3] B. C. Kelly,[3] S. M. Croom,[4] R. L. Webster,[5] E. Berger,[3] R. Chornock,[3] W. S. Burgett,[6] K. C. Chambers,[6] N. Kaiser[6] and P. A. Price[7]

[1]*Department of Physics, University of Western Cape, Bellville 7535, Cape Town, South Africa*
[2]*Department of Physics, Durham University, South Road, Durham DH1 3LE, UK*
[3]*Harvard–Smithsonian Center for Astrophysics, 60 Garden Street, Cambridge, MA 02138, USA*
[4]*Sydney Institute for Astronomy, School of Physics, The University of Sydney, NSW 2006, Australia*
[5]*School of Physics, University of Melbourne, Parkville, VIC 3010, Australia*
[6]*Institute for Astronomy, University of Hawaii at Manoa, Honolulu, HI 96822, USA*
[7]*Department of Astrophysical Sciences, Princeton University, Princeton, NJ 08544, USA*

Accepted 2013 May 21. Received 2013 May 21; in original form 2013 March 28

ABSTRACT

Over the past 20 years reverberation mapping has proved one of the most successful techniques for studying the local (<1 pc) environment of supermassive black holes that drive active galactic nuclei. Key successes of reverberation mapping have been direct black hole mass estimates, the radius–luminosity relation for the Hβ line and the calibration of single-epoch mass estimators commonly employed up to $z \sim 7$. However, observing constraints mean that few studies have been successful at $z > 0.1$, or for the more-luminous quasars that make up the majority of current spectroscopic samples, or for rest-frame ultraviolet emission lines available in optical spectra of $z > 0.5$ objects. Previously, we described a technique for stacking cross-correlations to obtain reverberation mapping results at high z. Here, we present the first results from a campaign designed for this purpose. We construct stacked cross-correlation functions for the C IV and Mg II lines and find a clear peak in both. We find that the peak in the Mg II correlation is at longer lags than C IV consistent with previous results at low redshift. For the C IV sample, we are able to bin by luminosity and find evidence for increasing lags for more-luminous objects. This C IV radius–luminosity relation is consistent with previous studies but with a fraction of the observational cost.

Key words: galaxies: active – quasars: emission lines – quasars: general – galaxies: Seyfert.

1 INTRODUCTION

The inner regions of active galactic nuclei (AGN) offer a unique opportunity to study matter within a few parsecs of a supermassive black hole (SMBH). Reverberation mapping is designed to study (primarily) the broad-line region (BLR) of AGN by measuring the interaction between continuum and broad-line flux variations (Blandford & McKee 1982; Peterson 1993). The physical model assumes the BLR is photoionized by a UV continuum that is emitted from a much smaller radius. Variations in the ionizing continuum produce correlated variations in the broad emission-line flux after a delay that can be associated with the light travel time.

Reverberation mapping of a single system requires many spectroscopic epochs of emission-line and continuum luminosity measurements. The time lag between continuum and emission-line variations is given by the peak in the cross-correlation between the two light curves. To date lags have been measured for nearly 50 objects following this approach.

Reverberation mapping has led to significant advances in the understanding of AGN [e.g. the radius–luminosity relation (Wandel, Peterson & Malkan 1999; Bentz et al. 2006), stratification and kinematics of the BLR (Peterson & Wandel 1999, 2000), black hole mass estimates (Peterson et al. 2004), etc.]. However, traditionally these campaigns have been observationally expensive as they require many observations of individual objects over a long period of time. Furthermore, these constraints have meant that even at moderate redshift ($z > 0.4$) there are no reverberation lags measured with the exception of one tentative result at $z = 2.2$ (Kaspi et al. 2007). This also means that, apart from some notable exceptions that have had multi-epoch UV spectroscopy, the vast majority of measured lags are for the Hβ line.

In a previous paper (Fine et al. 2012), we discussed the potential gains of combining extensively sampled time-resolved photometric

⋆E-mail: s.lb.fine@gmail.com

surveys, specifically the Panoramic Survey Telescope & Rapid Response System 1 (Pan-STARRS1) medium-deep survey (PS1 MDS), with relatively few epochs of spectroscopy on large samples of Quasi-Stellar Objects (QSOs). Current multi-object spectrographs make it possible to rapidly obtain spectra of many hundreds of QSOs. While individual objects may not have a well-sampled emission-line light curves, Fine et al. (2012) showed (in simulations at least) that reverberation lags could be recovered through stacking.

In this Letter, we present the first results from a multi-epoch spectroscopic survey of the PS1 MDS fields with the aim of measuring reverberation lags in stacked QSO samples. Throughout, we assume $H_0,\ \Omega_{\rm M},\ \Omega_\lambda = 70,\ 0.3,\ 0.7$.

2 DATA

In Fine et al. (2012), we discussed the sources of our data and their reduction. We only repeat the main points briefly here. See Fine et al. (2012) for a more detailed description.

2.1 PS1 light curves

The PS1 telescope (Hodapp et al. 2004) is performing a series of photometric surveys of the northern sky. The MDS offers the best opportunity for our analysis. Images of the 10 MDS fields are taken every four to five nights in the *grizy* bands while not affected by the Sun or Moon (Kaiser et al. 2010; Tonry et al. 2012). We use PSPHOT, part of the standard PS1 Image Processing Pipeline system (Magnier 2006), to extract point spread function photometry from nightly stacked images of the MDS fields. Each nightly stack is divided into ∼70 skycells. We calibrate each skycell separately using Sloan Digital Sky Survey (SDSS) photometry (Fukugita et al. 1996; York et al. 2000) of moderately bright ($16 <$ Mag. < 18.5) point sources (type $= 6$ in the SDSS data base). Each of the light curves is inspected for outliers that are removed manually, in total <1 per cent of the data points were removed.

2.2 Hectospectra

QSOs in the MDS fields are being observed for an ongoing project to study the variability of QSOs. QSO candidates are selected for spectroscopy using photometric data bases of QSOs (Richards et al. 2009; Bovy et al. 2011) to which we add point sources that correspond to X-ray sources, variability selected objects and ultraviolet excess (UVX)-selected objects.

We are surveying the MDS fields with the Hectospec instrument on the Multiple Mirror Telescope (MMT). Each MDS field is tiled with seven MMT pointings. Exposures are ∼1.5 h in length meaning that an MDS field (∼500 QSOs) can be surveyed in approximately one night of good-quality on-sky observing time. The spectra are extracted and reduced using standard Hectospec pipelines (Mink et al. 2007). They are then flux calibrated using observations of F stars in the same fields.

Spectra are classified and redshifted manually using the RUNZ code (Colless et al. 2001; Drinkwater et al. 2010). So far from 6.5 nights awarded we have observed 15 Hectospec fields (5 more than once). Further spectra were obtained from spare fibre allocations by the Pan-STARRS transient group. In total, we have spectra of 2727 objects, 1228 of which are QSOs, 368 of which have >1 spectroscopic epoch.

3 ANALYSIS

3.1 *K*-corrections

From the MDS we have *griz*-band light curves for each object in our sample. We *K*-correct these magnitudes using a simple model fitted to the SDSS *ugriz*-band magnitudes. We fit a power law along with a template for QSO emission lines and a Lyman α break (see e.g. Croom et al. 2009 for a similar if more detailed approach). While this model is not always a good fit to the SDSS magnitudes, it suffices for the purposes of interpolating *K*-corrections for this work.

We *K*-correct all of our light curves to a single rest wavelength (1350 and 3000 Å for C IV and Mg II, respectively). Note that the value of this *K*-correction affects any cross-covariance analysis. On the other hand cross-correlations are normalized and hence unaffected by the value of the *K*-correction (see Section 3.3).

3.2 Line flux measurements

In Fig. 1, we show the redshift distribution of the 368 QSOs with >1 spectrum. The distribution is relatively typical of optically selected QSO surveys with the majority between $z \sim 0.5$ and 3. Over this redshift range the strongest, and most heavily studied, broad emission lines are Mg II (λ2789) and C IV (λ1549). We will focus on these two lines throughout the rest of this work.

We fit the Mg II and C IV lines following the multiple-Gaussian prescription outlined in Fine et al. (2008, 2010) and each fit is manually inspected to check the reliability. Note that the standard Hectospec pipeline does not return a variance array for the spectra. However, from calculating the scatter in flat regions of the spectra it is clear that the spectral signal to noise (S/N) is $\gtrsim$10 pixel$^{-0.5}$ for the majority of sources. Errors on the emission-line fluxes are therefore dominated by flux calibration errors that we find to be ∼5–10 per cent by comparing the fibre magnitudes of calibration F stars with their SDSS photometry. Note that this will introduce correlated errors into our flux measurements since a single flux calibration is used for each Hectospec field.

Manual inspection was performed to remove bad fits, sky residuals, broad- and narrow-line absorption (in instances where narrow absorption lines or sky residuals did not significantly affect the emission line the effected pixels were simply masked and the line was fitted as normal) and other potential sources of contamination. The manual inspection was carried out several times with varying degrees of exclusivity. In general, we found that more exclusive selection (i.e. more objects thrown out) produced the highest fidelity in our results. After this procedure, we were left with 89 (Mg II) and

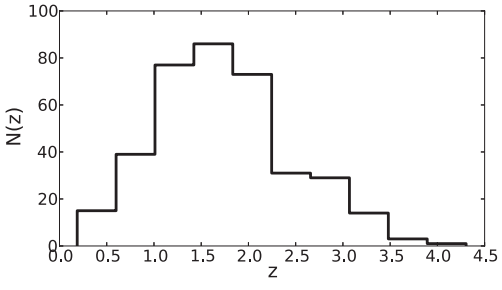

Figure 1. The redshift distribution of the 368 QSOs in our sample with more than one spectrum.

75 (C IV) objects with a good fit to their emission lines at more than one spectroscopic epoch.

3.3 Cross-correlation analysis

The correlation coefficient r for two samples (x, y) is

$$r(x, y) = \frac{\mathrm{Cov}(x, y)}{\sigma_x \sigma_y} = \sum_{i,\, j} \frac{(x_i - \overline{x})(y_j - \overline{y})}{\sigma_x \sigma_y}, \quad (1)$$

where $\mathrm{Cov}(x, y)$ is the covariance between the samples and σ is the rms of the samples. Fine et al. (2012) concentrated on cross-covariances rather than cross-correlations primarily because the rms of the emission-line fluxes is poorly constrained from just two measurements. In practice, we find it considerably more favourable to use cross-correlations in our analysis. We do this since QSO-to-QSO variations require normalization of the covariance function, and while the rms may not always be well defined, it does improve the quality of the stacked results. Nevertheless, most of the results presented here for cross-correlations are visible, if with decreased clarity, in the covariance functions as well. Furthermore, cross-correlations are not susceptible to the step-biases we found in cross covariances in Fine et al. (2012).

To calculate the stacked cross-correlations, we take each emission-line flux/continuum photometric observation pair for each object in our sample. We calculate the time lag τ between them and the individual ith, jth term of equation (1). We bin all of the emission line–continuum data–data pairs by their lag and average over all pairs within a bin to create the stack.

In practice, we tried mean, variance-weighted and median stacks. Each of these methods produced roughly equivalent results for the C IV stack. For Mg II, we found that variance weighting gave the highest S/N in the cross-correlation. Given the sparsity of solid reverberation-mapping results at $z > 0.3$, this Letter's primary goal is to identify a(any) peak in the stacked correlation functions presented here. The variance-weighted mean biases the results towards the higher quality data (in practice the brighter objects) and has the effect of reducing the noise in the final stack. Because we find that it gives the clearest results for Mg II, we will use the variance-weighted mean to create our stacked correlation functions throughout this Letter.

To estimate errors on the stacks, we use the field-to-field technique whereby we divided our sample into nine subsamples. We then calculated the stacked cross-correlation functions in each subsample and took the rms of the subsamples divided by $\sqrt{9} = 3$ as an estimate of the error.

3.4 Randomized analysis

As a check on the significance of any results, we obtain we also performed a randomized analysis. For this, we take the spectroscopic flux measurements for each individual object and replace them with random values drawn from a Gaussian distribution with the same mean and rms as the observations (note that in most cases the mean and rms are only defined by two observations). We then perform the same stacked cross-correlation analysis with the observed photometric light curves. This process was repeated 200 times and the mean and rms of the separate realizations was recorded for comparison with our results.

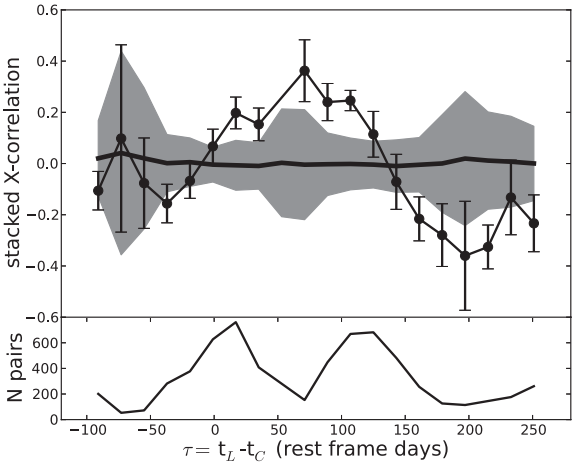

Figure 2. The stacked C IV cross-correlation for all objects with >1 good emission-line measurement. The thick line and shaded region shows the mean and rms of the random simulations we performed. In the bottom panel, we show the number of continuum/emission-line flux pairs that go into the stack at each point (i.e. the number summed over in equation 1).

4 RESULTS

4.1 The full C IV stack

Fig. 2 shows the variance-weighted stacked cross-correlation function for all 75 objects with more than one epoch of C IV data. The lower panel in the plot shows the number of data–data pairs that contribute to the stack in each τ bin. Since PS1 surveys the MD07 field for approximately six months of each year, we sample lags of $0.5 \pm$ an integer years poorly. Once transformed to rest-frame time delays, this creates the peaks in the N pairs distribution.

Each object in the C IV sample will have a different lag for its C IV line due to a variety of reasons, perhaps most importantly their different luminosities. The C IV sample spans $37.5 < \log_{10}\lambda L_\lambda(1350) < 39.5$ assuming $\tau \propto L^{0.5}$ this gives a potential factor-of-10 range in lags within our sample. The effect of stacking objects with a broad range of lags would be to smooth our results. Despite this potential smoothing, we find a significant peak in the cross-correlation function in Fig. 2. The solid line and shaded area in the figure show the mean and rms from our 200 simulated cross-correlations where we randomize the spectroscopic flux measurements (Section 3.4). Seven of our cross-correlation points lie above the rms level (and five below) indicating a significant correlation between our photometric and spectroscopic data sets.

4.2 Towards a radius–luminosity relation for C IV

To reduce the smoothing caused by the range of lags in each stack, and to aim towards a more useful result to the community (measuring the r–L relation for C IV), we bin the sample by the i-band absolute magnitude. Fig. 3 shows the stacked cross-correlation for three equal size (in terms of number of objects) magnitude bins.

There is some evidence for a peak in the two brighter bins, and perhaps in the faintest as well. There is also a suggestion that the peak is shifting towards longer lags in the more-luminous bins. To quantify this, we fitted offset Gaussian functions to each of the cross-correlations. In Fig. 4, we plot the centroid of the fitted Gaussian against the mean continuum luminosity at 1460Å for each bin. Error bars in Fig. 4 come from the Gaussian fit for $\tau_{\rm fit}$ and the rms of the continuum luminosities for λL_λ. The grey lines in the

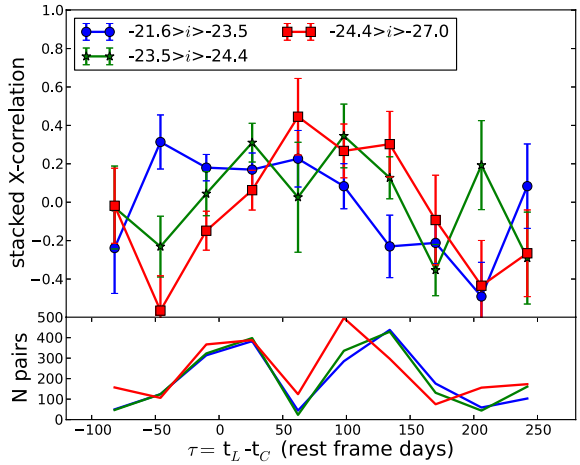

Figure 3. The stacked C IV cross-correlation for three magnitude bins with equal numbers of objects.

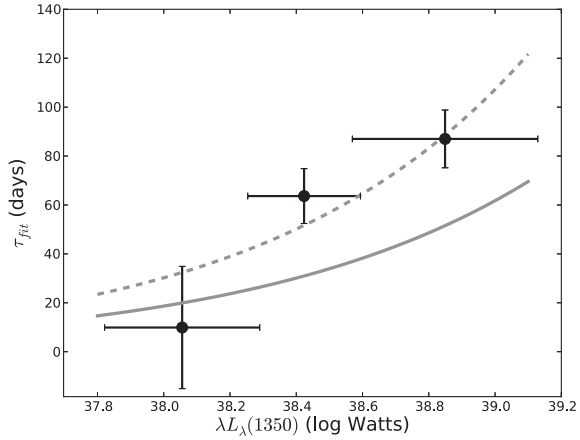

Figure 4. The *r–L* relation for the C IV line where $\tau_{\rm fit}$ is derived from Gaussian fits to the data in Fig. 3. The grey solid and dashed lines give the Kaspi et al. (2007) FITEXY and BCES fits to their *r–L* relation, respectively.

figure represent the two fits Kaspi et al. (2007) present for their C IV *r–L* relation.

There are competing biases that effect the location of the peak in our stacked cross-correlations. For example, brighter objects tend to have higher S/N photometry and spectroscopy giving them more weight in the variance-weighted mean stacks. On the other hand, fainter QSOs tend to be more variable potentially increasing their impact on the stacks. Although more data are clearly needed to determine its exact form, there is tantalizing evidence for the existence of a C IV radius luminosity relation.

4.3 The Mg II correlation

While the Mg II sample is slightly larger than C IV, we do not find that this translates to a more signal in the stacked correlation function. However, in the full variance-weighted stack, we do find a clear peak. The stacked correlation for the Mg II sample is given in Fig. 5 along with the C IV stack for comparison. The heavy line and shaded area in the figure show the mean and rms from our 200 simulated cross-correlations where we randomize the Mg II flux measurements. Again, a significant peak is evident in the Mg II cross-correlation.

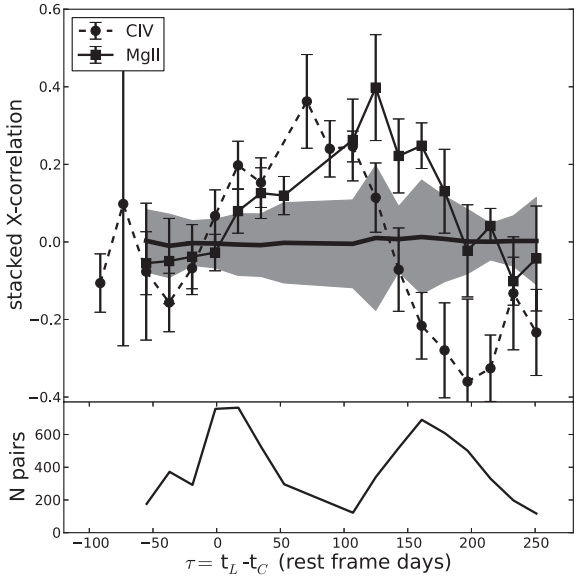

Figure 5. Solid: the stacked cross-correlations for the whole Mg II sample. The dashed line shows the C IV results and the heavy line and shaded region show the mean and rms from our random simulations (Section 3.4).

The location of the Mg II peak is at considerably longer lags than for C IV. This is consistent with results for low-redshift objects where higher ionization lines such as C IV exhibit shorter lags. We note, however, that in our sample the situation is complicated by the fact that the Mg II sample is by necessity lower redshift than the C IV, hence the objects contributing to the stack tend to be less luminous which will bias the Mg II lag with respect to the high-z, luminous C IV sample. We have tried splitting up the Mg II sample into magnitude bins to investigate any *r–L* relationship but find no convincing peaks when binned.

5 DISCUSSION

Reverberation mapping results are the basis for a large part of our understanding of AGN. With some notable exceptions the vast majority of SMBH mass estimates for AGN come directly or indirectly from reverberation mapping. In particular, single-epoch estimators (McLure & Jarvis 2002; Vestergaard 2002), that have been applied to >100 000 objects have their basis in reverberation mapping, rely on the *r–L* relation and are calibrated against reverberation masses.

As of yet there is no published *r–L* relation for the Mg II line. Kaspi et al. (2007) present a relation for the C IV line based on the six objects that have had a reverberation lag measured for them. However, of these objects, four have very similar luminosities and cannot be used to define the gradient of the relation. Their gradient is defined mostly by their results for S5 0836+71, the only high-redshift QSO to have a lag measured, and the dwarf Seyfert NGC 4395, an extremely underluminous AGN (Peterson et al. 2005).

In this Letter, we present the first results from our campaign to derive reverberation signals from stacks of objects. The technique naturally lends itself to the mapping of rest-frame ultraviolet lines (Mg II and C IV) at high redshift. We show that from the 75 objects in our C IV stack we get a clear peak in the cross-correlation. When binned by luminosity there may be some evidence for an *r–L* relation although our data are not well constrained. However, our data are in good agreement with the C IV *r–L* relation from Peterson et al. (2005) and (Kaspi et al. 2007). While still at an early stage, the

consistency of the Peterson results at $z \sim 0$, ours at $z \sim 2$, and Kaspi's at $z = 2.2$ appears to indicate little evolution in the *r–L* relation with redshift.

We also find a peak in the stacked Mg II sample. Comparing with the C IV results, we find the Mg II peak to be at larger τ, indicative of a stratified BLR as observed in low-redshift objects. However, our Mg II and C IV samples are at different redshifts, with different luminosity distributions confusing a direct comparison.

6 CONCLUSIONS

We have shown that by stacking samples of QSOs that have continuous photometric monitoring and two-or-more spectra it is possible to recover a reverberation-mapping time lag. We give stacked cross-correlations for both the Mg II and C IV lines and find a clear peak in both. The Mg II peak is at considerably longer lags indicative of stratification of the BLR. Furthermore, when binned by luminosity the C IV sample shows evidence for increasing lags with increasing luminosity. From these data, we make an initial *r–L* plot for the C IV line. Although we caution that our relation is effected by significant biases, we find it is consistent with previous evaluations.

This Letter demonstrates the potential of the stacking technique to produce reverberation-mapping results at high redshift. Potentially this technique could provide an avenue towards answering some key questions about high-redshift AGN. However, it is clear that more data are required before strong constraints can be derived from this technique.

ACKNOWLEDGEMENTS

SF would like to acknowledge SKA South Africa and the NRF for their funding support. The data presented in this work came from the Pan-STARRS1 telescope and the Multiple Mirror Telescope. Observations reported here were obtained at the MMT Observatory, a joint facility of the Smithsonian Institution and the University of Arizona. The Pan-STARRS1 Surveys (PS1) have been made possible through contributions of the Institute for Astronomy, the University of Hawaii, the Pan-STARRS Project Office, the Max-Planck Society and its Participating Institutes, the Max Planck Institute for Astronomy, Heidelberg and the Max Planck Institute for Extraterrestrial Physics, Garching, The Johns Hopkins University, Durham University, the University of Edinburgh, Queen's University Belfast, the Harvard–Smithsonian Center for Astrophysics, the Las Cumbres Observatory Global Telescope Network Incorporated, the National Central University of Taiwan, the Space Telescope Science Institute, and the National Aeronautics and Space Administration under Grant No. NNX08AR22G issued through the Planetary Science Division of the NASA Science Mission Directorate.

REFERENCES

Bentz M. C., Peterson B. M., Pogge R. W., Vestergaard M., Onken C. A., 2006, ApJ, 644, 133
Blandford R. D., McKee C. F., 1982, ApJ, 255, 419
Bovy J. et al., 2011, ApJ, 729, 141
Colless M. et al., 2001, MNRAS, 328, 1039
Croom S. M. et al., 2009, MNRAS, 399, 1755
Drinkwater M. J. et al., 2010, MNRAS, 401, 1429
Fine S. et al., 2008, MNRAS, 390, 1413
Fine S., Croom S. M., Bland-Hawthorn J., Pimbblet K. A., Ross N. P., Schneider D. P., Shanks T., 2010, MNRAS, 409, 591
Fine S. et al., 2012, MNRAS, 427, 2701
Fukugita M., Ichikawa T., Gunn J. E., Doi M., Shimasaku K., Schneider D. P., 1996, AJ, 111, 1748
Hodapp K. W. et al., 2004, in Oschmann J. M., Jr, ed., Proc. SPIE Vol. 5489, Optical Design of the Pan-STARRS Telescopes. SPIE, Bellingham, p. 667
Kaiser N. et al., 2010, in Stepp L. M., Gilmozzi R., Hall H. J., eds, Proc. SPIE Vol. 7733, Ground-based and Airborne Telescopes III. SPIE, Bellingham, p. 77330E
Kaspi S., Brandt W. N., Maoz D., Netzer H., Schneider D. P., Shemmer O., 2007, ApJ, 659, 997
Magnier E., 2006, in Ryan S., ed., Advanced Maui Optical and Space Surveillance Technologies Conference, The Pan-STARRS PS1 Image Processing Pipeline. The Maui Economic Development Board, Maui, Hawaii, p.e50
McLure R. J., Jarvis M. J., 2002, MNRAS, 337, 109
Mink D. J., Wyatt W. F., Caldwell N., Conroy M. A., Furesz G., Tokarz S. P., 2007, in Shaw R. A., Hill F., Bell D. J., eds, ASP Conf. Ser. Vol. 376, Automating Reduction of Multifiber Spectra from the MMT Hectospec and Hectochelle. Astron. Soc. Pac., San Francisco, p. 249
Peterson B. M., 1993, PASP, 105, 247
Peterson B. M., Wandel A., 1999, ApJ, 521, L95
Peterson B. M., Wandel A., 2000, ApJ, 540, L13
Peterson B. M. et al., 2004, ApJ, 613, 682
Peterson B. M. et al., 2005, ApJ, 632, 799
Richards G. T. et al., 2009, ApJS, 180, 67
Tonry J. L. et al., 2012, ApJ, 745, 42
Vestergaard M., 2002, ApJ, 571, 733
Wandel A., Peterson B. M., Malkan M. A., 1999, ApJ, 526, 579
York D. G. et al., 2000, AJ, 120, 1579

This paper has been typeset from a TEX/LATEX file prepared by the author.